MITSUBISHI ELECTRIC RESEARCH LABORATORIES
https://www.merl.com

# Sequential linearization-based station keeping with optical navigation for NRHO

Elango, Purnanand; Di Cairano, Stefano; Berntorp, Karl; Weiss, Avishai

TR2022-114 September 29, 2022

**Abstract**

In recent years, fuel-efficient station-keeping techniques have been developed for the planned Lunar Gateway mission to a near rectilinear halo orbit (NRHO). Station-keeping approaches that rely on an autonomous navigation system that doesn't require communications with Earth are particularly important for ensuring safety and reliability. This paper presents a targeting approach for NRHO station keeping based on sequential linearization and evaluates its performance in a closed- loop simulation with a state estimator that receives position measurements from horizon-based optical navigation (OPNAV). Simulation results indicate an annual station-keeping cost (delta-v) of about 1.14 m s-1 for the proposed OPNAV-based station keeping.

*AAS/AIAA Astrodynamics Specialist Conference 2022*



Mitsubishi Electric Research Laboratories, Inc.
201 Broadway, Cambridge, Massachusetts 02139

AAS 22-844

# SEQUENTIAL LINEARIZATION-BASED STATION KEEPING WITH OPTICAL NAVIGATION FOR NRHO

**Purnanand Elango[*], Stefano Di Cairano[†], Karl Berntorp[‡], and Avishai Weiss[§]**

In recent years, fuel-efficient station-keeping techniques have been developed for the planned Lunar Gateway mission to a near rectilinear halo orbit (NRHO). Station-keeping approaches that rely on an autonomous navigation system that doesn't require communications with Earth are particularly important for ensuring safety and reliability. This paper presents a targeting approach for NRHO station keeping based on sequential linearization and evaluates its performance in a closed-loop simulation with a state estimator that receives position measurements from horizon-based optical navigation (OPNAV). Simulation results indicate an annual station-keeping cost (delta-v) of about $1.14$ m s$^{-1}$ for the proposed OPNAV-based station keeping.

## INTRODUCTION

The upcoming Lunar Orbital Platform-Gateway (LOP-G)[1,2] will be deployed on a 9:2 resonant near-rectilinear halo orbit (NRHO) around the Earth-Moon $L_2$ point.[3,4] The ideal 9:2 NRHO is a closed, periodic solution to the Earth-Moon circular-restricted three-body-problem (CR3BP). However, the CR3BP does not consider the gravitational influence of celestial bodies other than Earth and Moon, does not make use of the true positions of the celestial bodies with respect to a time epoch, i.e., ephemeris information, nor does it account for higher-order effects on spacecraft dynamics, e.g., solar radiation pressure (SRP) and Moon J2 harmonics. To keep station-keeping fuel consumption as low as possible, a high-fidelity trajectory near the ideal NRHO that accounts for such realistic effects may be computed and used as a baseline trajectory for the LOP-G.[3] See Figure 1 for an example of such a baseline. The baseline trajectory is aperiodic, of finite length, and unstable. Since deviations from the baseline are unavoidable due to navigational uncertainty, station keeping is required.

The recently launched CAPSTONE mission will be the first spacecraft to fly on an NRHO to verify the dynamics of the orbit and validate station-keeping strategies under real conditions.[5] Shortly after trans-lunar injection, CAPSTONE lost communication with NASA's Deep Space Network (DSN), jeopardizing the mission.[6] While the spacecraft eventually regained communication,[7] such events highlight the possibility of communication faults and the need for backup autonomous navigation solutions that do not rely on DSN. Furthermore, in the coming years, NRHO will see a host of spacecraft, both crewed and uncrewed, arriving to build LOP-G, supply and service it, and use it

[*]Ph.D. Student, Department of Aeronautics and Astronautics, University of Washington, Seattle, WA 98195. E-mail: pelango@uw.edu. P. Elango interned at MERL during the development of this work.
[†]Distinguished Research Scientist, Mitsubishi Electric Research Laboratories (MERL), Cambridge, MA 02139.
[‡]Senior Principal Research Scientist, Mitsubishi Electric Research Laboratories (MERL), Cambridge, MA 02139.
[§]Principal Research Scientist, Mitsubishi Electric Research Laboratories (MERL), Cambridge, MA 02139.

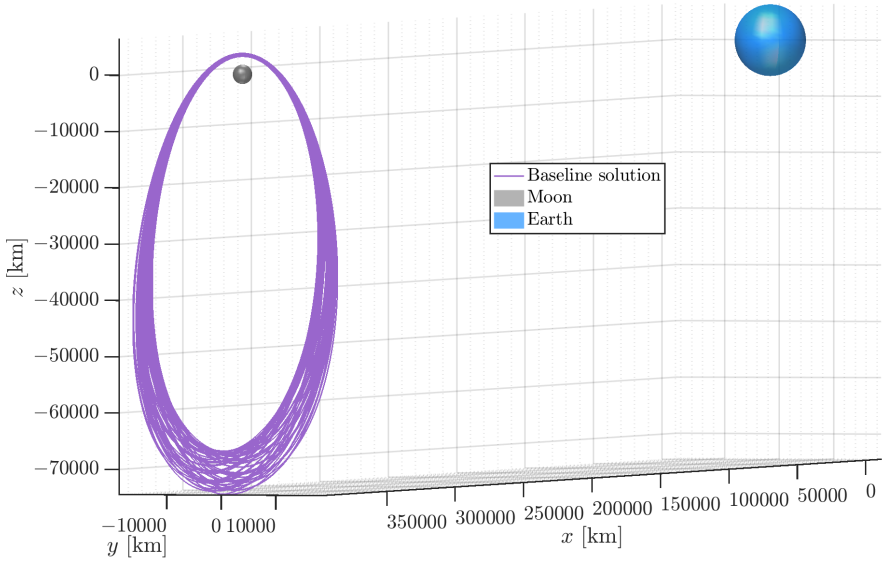


**Figure 1**: An NRHO solution represented in the Earth-Moon rotating frame $\mathrm{F_S}$ computed in the high-fidelity ephemeris model via multiple shooting. The solution consists of 60 revolutions around the Moon spanning 394 days.

as a launching pad for missions to the lunar surface or out to Mars. Given the increased activity, DSN-based navigation services will need to be rationed. As such, there is a need for alternatives. The Lunar GNSS Receiver Experiment (LuGRE) will attempt to use GPS and Galileo signals in the lunar environment and on the lunar surface,[8] and CAPSTONE will be testing a new peer-to-peer autonomous navigation system that measures range and range-rate relative to NASA's Lunar Reconnaissance Orbiter (LRO).[5]

Horizon-based optical navigation (OPNAV) is another candidate technology that has recently matured and will be demonstrated on the upcoming Artemis 1 mission, currently slated for launch later this summer.[9] OPNAV is a fully onboard solution that can be deployed in the vicinity of any planet or moon.

In this work, we develop an autonomous station-keeping approach for NRHO that relies on state estimates generated from OPNAV measurements. In recent years, many strategies for station-keeping on high-fidelity NRHOs have been proposed.[10–20] Such strategies are generally categorized into short-horizon maneuvering, which maintains a spacecraft near an existing baseline, and long-horizon maneuvering, which transitions from one baseline trajectory to another. Using both short- and long-horizon maneuvering enables indefinite station-keeping on NRHOs.[17] Short-horizon maneuvering is further categorized into spectrum-based strategies that align a spacecraft with the stable subspace near the baseline,[20–22] and target point approaches that control the spacecraft state or a portion of the state to attain a desired value at some future time, see e.g., $x$-axis crossing control.[14,21] Target point methods can also be used for long-horizon maneuvering. While long-horizon maneuvers may solve an optimal control problem to transition between two pre-computed baseline trajectories,[17] when used for long-horizon maneuvers, target point methods do not require a pre-computed baseline to transition to, but rather generate the baseline trajectory in real-time.[10]

We introduce a variant of the long-horizon $x$-axis crossing control method based on sequential linearization. We use the method in a receding-horizon approach that obviates the need for short-

horizon station-keeping.[14] That is, instead of generating a baseline trajectory offline or computing one in real time and then using short-horizon maneuvers to maintain the spacecraft near the baseline, long-horizon maneuvers are computed after each revolution to maintain the spacecraft near an NRHO. Every apolune, the algorithm checks whether the $x$-component of the predicted spacecraft velocity at perilune relative to the Earth-Moon rotating frame six and half revolutions downstream is beyond a threshold, and if so, triggers the computation of a long-horizon maneuver to ensure the threshold will be satisfied. The long-horizon maneuver is computed based on sequentially linearizing the predicted trajectory. A linear approximation of the high-fidelity nonlinear dynamics is iteratively used to determine a velocity impulse which ensures the desired target velocity is achieved by the nonlinear system. The proposed approach is closely related to the sequential convex programming algorithms specialized to trajectory optimization[23] where the nonlinear dynamics is linearized about an iteratively updated reference trajectory.

We demonstrate the robustness of this baseline-free station-keeping strategy on NRHO to state estimates generated by an extended Kalman filter (EKF) that gets OPNAV position measurements from a high-fidelity ephemeris-based simulation and the synthetic rendering software Basilisk[24] and Vizard.[25] To the authors' knowledge, only a few other past works[12,26–29] have demonstrated realistic closed-loop station-keeping simulations with OPNAV, and this work may be the first to do so on NRHO with implementation details.

The rest of the paper is organized as follows. First we introduce the spacecraft and control model along with the high-fidelity model for NRHO. We then provides details on horizon-based optical navigation and the extended Kalman filter. Next, we describe the sequential linearization-based targeting approach for NRHO station keeping. We then demonstrate the performance of the approach in a closed-loop station-keeping simulation with OPNAV. Finally, concluding remarks are provided.

## SPACECRAFT MODEL

Consider a point-mass spacecraft in cis-lunar space and the synodic frame $\mathrm{F_S}$. The frame $\mathrm{F_S}$ is a non-inertial rotating frame with its $x$-axis pointing from the Earth-Moon barycenter towards the center of mass of the Moon and its $z$-axis along the angular momentum vector of the Earth-Moon system in the CR3BP. This frame is commonly chosen for the analysis of NRHOs since it is useful for observation and communication from Earth [30, Section 2.1.2]. The nonlinear equation of motion of the spacecraft is given by

$$\dot{\theta}(t) = g(t, \theta(t), u(t)), \tag{1}$$

where $\theta \triangleq [r^\top \ v^\top]^\top$ is the state vector, $r$ is the position of the spacecraft with respect to the Earth-Moon barycenter resolved in $\mathrm{F_S}$, $v \triangleq \dot{r}$ is the velocity of the spacecraft with respect to $\mathrm{F_S}$ resolved in $\mathrm{F_S}$, and $u$ is the control vector of thrust forces acting on the spacecraft, resolved in $\mathrm{F_S}$. The right-hand-side of the model in (1) accounts for the major predictable external forces acting on the spacecraft, see [31, Section 2.3] for further details.

We assume that the spacecraft is actuated with impulsive thrusters, wherein a thrust impulse is modeled to cause an instantaneous change in the velocity of the spacecraft. Consider the motion of the spacecraft in the time interval $[t_1, t_2]$ with a thrust impulse $\zeta \in \mathbb{R}^3$ applied at $t' \in (t_1, t_2)$. The control input $u(t)$ can be represented as

$$u(t) = \begin{bmatrix} 0_3 \\ \zeta \end{bmatrix} \delta(t - t'), \tag{2}$$

for $t \in [t_1, t_2]$, where $\delta(t)$ is the Dirac delta function. The right-hand-side of (1) can be rewritten as

$$g(t, \theta(t), u(t)) = f(t, \theta(t)) + u(t), \tag{3}$$

for $t \in [t_1, t_2]$, where $f$ includes the previously mentioned external forces acting on the spacecraft. The (uncontrolled) natural motion of the spacecraft is thus given by

$$\dot{\theta}(t) = f(t, \theta(t)). \tag{4}$$

The spacecraft state at $t_2$ obtained after the impulse at $t'$ is

$$\begin{aligned} \theta(t_2) &= \theta(t_1) + \int_{t_1}^{t_2} g(\tau, \theta(\tau), u(\tau)) \mathrm{d}\tau, \\ &= \theta(t_1) + \int_{t_1}^{t_2} \left( \begin{bmatrix} 0_3 \\ \zeta \end{bmatrix} \delta(\tau - t') + f(\tau, \theta(\tau)) \right) \mathrm{d}\tau, \\ &= \theta(t') + \int_{t'}^{t_2} f(\tau, \theta(\tau)) \mathrm{d}\tau, \end{aligned} \tag{5}$$

where

$$\theta(t') = \theta(t_1) + \begin{bmatrix} 0_3 \\ \zeta \end{bmatrix} + \int_{t_1}^{t'} f(\tau, \theta(\tau)) \mathrm{d}\tau. \tag{6}$$

While the propagation of spacecraft dynamics with impulsive thrust (6) is used in the subsequent development, with minor modifications it can be adapted to handle thrust pulses of finite-duration. Note that finite-duration thrust pulses on the order of minutes can be approximated fairly well by thrust impulses due to the slow time scales of the system dynamics (4) on NRHO, especially near apolune.

A solution to (4) spanning a year is computed using multiple-shooting and is shown in Figure 1.

## HORIZON-BASED OPTICAL NAVIGATION

This work considers horizon-based OPNAV as an autonomous backup navigation strategy for spacecraft station keeping on NRHO, which does not rely on external measurements and communication, e.g. range and range-rate measurements from the Deep Space Network (DSN). We can measure (estimate) the spacecraft position in the Moon-centered inertial frame using the OPNAV algorithm in [32, Figure 5], which is based on detecting the lit limb on the horizon of the Moon using an image taken by an onboard camera. This technique also provides the covariance associated with the position measurement [32, Figure 6]. The position measurement and the covariance can be transformed to the synodic frame $\mathrm{F_S}$.

To demonstrate closed-loop station keeping with realistic OPNAV we used the astrodynamics simulation and visualization software Basilisk[24] and Vizard.[25] Given a time epoch and the true position of the spacecraft, Basilisk can query the instantaneous positions of Sun, Earth, and Moon from the DE 421 ephemeris,[33] and call Vizard to render them along with the spacecraft in an appropriate frame. A pin-hole camera of desired field of view can be attached to the spacecraft, which can be oriented to point to the Moon. Vizard is capable of accurately capturing the illumination of the Moon due to the Sun in the view from the spacecraft, particularly the lit limb on the Moon horizon, which is a key aspect contributing to the realism of our closed-loop simulator. Moreover, the Vizard camera can simulate commonly observed distortions in images taken from spacecraft. Figure

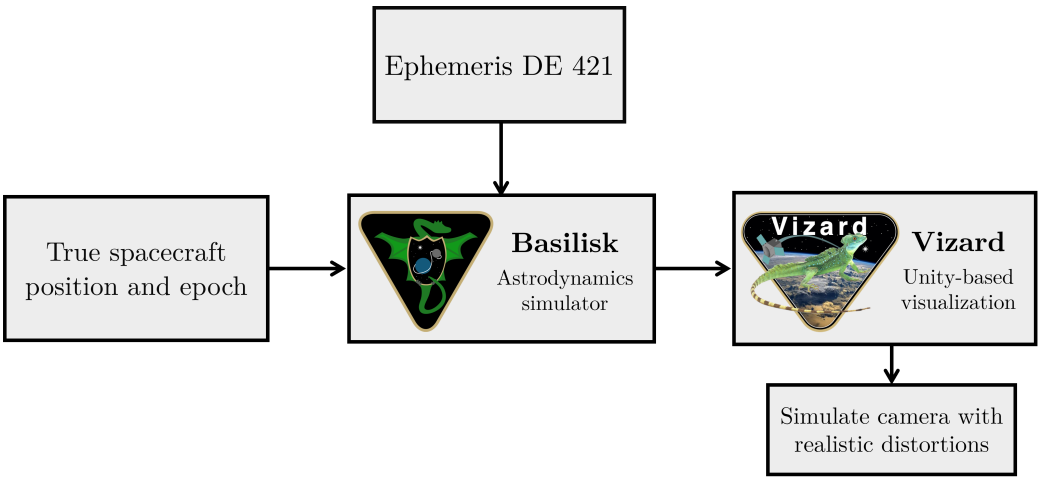


**Figure 2**: Flowchart describing how realistic images of the Moon are acquired from a simulated onboard camera.

2 illustrates this Basilisk-Vizard pipeline for acquiring Moon images. The limb points on the image of the Moon captured by the spacecraft camera are detected via the Canny transform[34] implemented in OpenCV,[35] and then used in the OPNAV algorithm [32, Figure 5] to measure (estimate) the spacecraft position.

Figure 3 shows the Vizard windows initialized by Basilisk when the spacecraft is near apolune and perilune. The limb points detected by the Canny transform from the two instances in Figure 3 are shown in Figure 4.

In our closed-loop simulation we use images of constant resolution ($2048 \times 2048$ pixels) at all times. Since the computational cost of the OPNAV algorithm is very dependent on the image resolution, we prefer not to vary the resolution of the image captured at different regions of the NRHO trajectory. Since the perilune and apolune of the NRHO are situated at about 3200 km and 70000 km, respectively, to ensure that the Moon occupies roughly the same fraction of area in all camera images, the field of view $\mathcal{F}$ of the camera is varied as follows

$$\mathcal{F} = \min\left\{2.8\arctan\left(\frac{R_{\text{Moon}}}{d_{\text{Moon}}(t)}\right), \frac{5\pi}{12}\right\} \text{ rad}, \tag{7}$$

where $R_{\text{Moon}}$ is the mean volumetric radius of the Moon, and $d_{\text{Moon}}(t)$ is the distance between the spacecraft and the Moon. This means that $\mathcal{F}$ ranges between $3^\circ$ to $78^\circ$ as the spacecraft moves from apolune to perilune.

The OPNAV measurement error is empirically observed to range between 2 and 20 km. The large variation in $\mathcal{F}$ causes the OPNAV measurement covariance computed according to [32, Section V] to be inconsistent with the observed measurement error, especially near perilune where $\mathcal{F}$ is large. This inconsistency is a combined effect of the large variation in $\mathcal{F}$ and a potential mismatch in modelling the geometry of the Moon between the OPNAV algorithm and the CAD model of the Moon used in Vizard. Since Moon's oblateness is not very pronounced, we assume that it is a perfect sphere with radius $R_{\text{Moon}} = 1737.4$ km (mean volumetric radius) in [32, Eq. 6] of the OPNAV algorithm. In a real mission, we could use a very high resolution camera with constant field of view. This will ensure that limb detection at apolune is reliable even if the Moon occupies a small fraction of the image.


(a) Spacecraft at perilune.

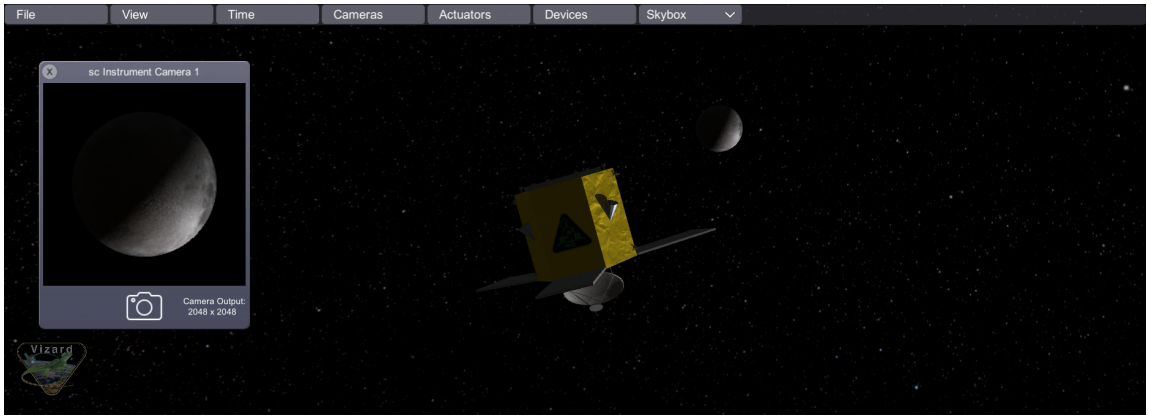


(b) Spacecraft at apolune.

**Figure 3**: Vizard renderings of the Moon and the spacecraft at a perilune and an apolune of a baseline NRHO solution. The windows on the left of each screen-capture show the image of the Moon taken by the spacecraft camera. Vizard renders the realistic lighting conditions of the Moon (as seen by the spacecraft at a given time epoch) based on the positions of Sun, Earth and Moon received from the DE 421 ephemeris via Basilisk.

Furthermore, if the Moon is imaged at intervals of a few hours, the onboard computers will have sufficient time to operate on the high resolution image of the Moon to extract the OPNAV position measurement. Therefore, in our simulation we scale the measurement covariance from the OPNAV algorithm [32, Figure 6] to ensure that its maximum eigenvalue is at least 16. This ensures that the state estimator will not excessively trust the OPNAV measurements. Future work will examine improvements to the simulation framework that allow greater reliance on the OPNAV measurement covariance.

### State Estimation

We use an EKF[36] to estimate the spacecraft state from the OPNAV position measurements. The true state of the spacecraft at the sampling time $t_j$, for some $j \in \mathbb{N}$, is

$$\theta_j = \theta_{j-1} + \int_{t_{j-1}}^{t_j} f(\tau, \theta(\tau))\, \mathrm{d}\tau, \tag{8}$$

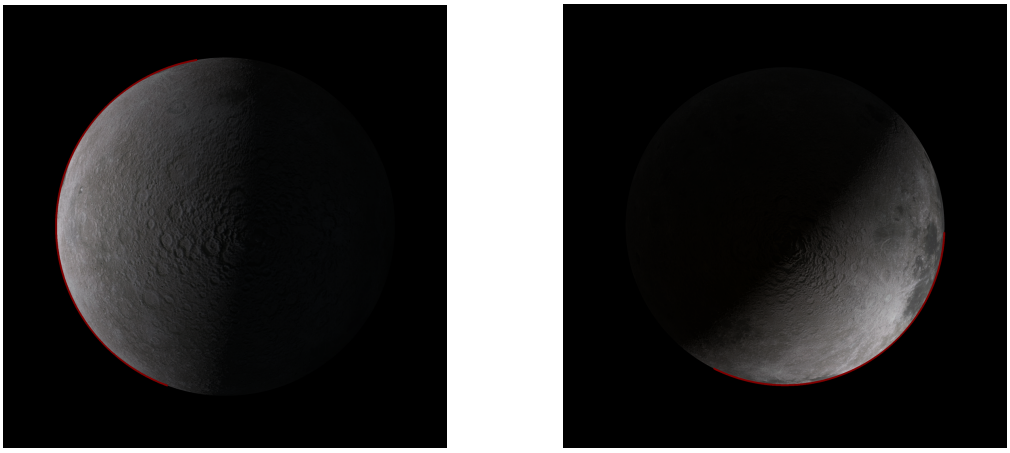

(a) Camera image at perilune.

(b) Camera image at apolune.

**Figure 4**: The lit limb (marked in red) detected by the Canny transform performed on the spacecraft camera images from Figure 3.

where the true initial state is $\theta(t_0) = \theta_0$. The prediction of the state and covariance at time $t_j$ given the measurements until time $t_{j-1}$ is

$$\widehat{\theta}_{j|j-1} = \widehat{\theta}_{j-1|j-1} + \int_{t_{j-1}}^{t_j} f\big(\tau, \widehat{\theta}_{j-1}(\tau)\big)\,\mathrm{d}\tau, \tag{9a}$$

$$\Sigma_{j|j-1} = \Phi(t_j, t_{j-1})\Sigma_{j-1|j-1}\Phi(t_j, t_{j-1})^\top + Q_{j-1}, \tag{9b}$$

where $\widehat{\theta}_{j-1}(\tau)$ is the predicted state for $\tau \in [t_{j-1}, t_j]$ with $\widehat{\theta}_{j-1}(t_{j-1}) = \widehat{\theta}_{j-1|j-1}$, and the state transition matrix (STM) $\Phi(t_j, t_{j-1})$ is given by integrating the matrix differential equation

$$\dot{\Phi}(\tau, t_{j-1}) = \left( \left.\frac{\partial f(\gamma, \theta)}{\partial \theta}\right|_{\left(\tau, \widehat{\theta}_{j-1}(\tau)\right)} \right) \Phi(\tau, t_{j-1}), \tag{10}$$

over the time interval $[t_{j-1}, t_j]$ with $\Phi(t_0, t_0) = I_6$. In (9b) the STM computed for the predicted trajectory is used to propagate the state covariance. Although there is no mismatch between the actual system dynamics and the system model used in the filter, we introduce process noise to tune the estimator to account for potential model mismatch in the measurement equation*. We assume the following form of the process noise covariance (9b),

$$Q_j = \begin{bmatrix} q_r^2 I_3 & 0_{3\times 3} \\ 0_{3\times 3} & q_v(t_j)^2 I_3 \end{bmatrix}, \tag{11}$$

where

$$q_v(t_j) = q_{v,\mathrm{a}} \left| \frac{\widehat{d}_{\mathrm{Moon}}(t_j) - d_{\mathrm{Moon,p}}}{d_{\mathrm{Moon,a}} - d_{\mathrm{Moon,p}}} \right| + q_{v,\mathrm{p}} \left| \frac{d_{\mathrm{Moon,a}} - \widehat{d}_{\mathrm{Moon}}(t_j)}{d_{\mathrm{Moon,a}} - d_{\mathrm{Moon,p}}} \right|, \tag{12}$$

*Note that we do not account for the highly nonlinear mapping between the Moon image and the OPNAV position measurement described in [32, Figure 5].

with $q_{v,\text{a}} = 0.05$ cm s$^{-1}$, $q_{v,\text{p}} = 0.5$ cm s$^{-1}$, $q_r = 0.5$ km, $d_{\text{Moon,a}} = 71000$ km, $d_{\text{Moon,p}} = 3200$ km, and the predicted distance to Moon denoted by $\widehat{d}_{\text{Moon}}(t_j)$. Since the performance of the station-keeping approach is strongly dependent on the accuracy of the velocity estimates, we prescribe $q_v$ as a function of $\widehat{d}_{\text{Moon}}$ to account for the order of magnitude difference between the apolune speed ($\sim 0.1$ km s$^{-1}$) and the perilune speed ($\sim 1.6$ km s$^{-1}$).

The OPNAV position measurement at time $t_j$ entering the filter is denoted by

$$\beta_j = E_r \theta_j + \nu_j, \tag{13}$$

where $\nu_j \sim \mathcal{N}(\overline{\nu}_j, R_j)$ with mean $\overline{\nu}_j$ and covariance $R_j$, and

$$E_r = \begin{bmatrix} I_3 \\ 0_{3\times 3} \end{bmatrix}.$$

Finally, the correction step of the filter for obtaining the optimal state estimate and covariance at time $t_j$ is given by

$$K_j = \Sigma_{j|j-1} E_r^\top \left( E_r \Sigma_{j|j-1} E_r^\top + R_j \right)^{-1}, \tag{14a}$$

$$\widehat{\theta}_{j|j} = \widehat{\theta}_{j|j-1} + K_j(\beta_j - E_r \widehat{\theta}_{j|j-1}), \tag{14b}$$

$$\Sigma_{j|j} = (I - K_j E_r)\Sigma_{j|j-1}, \tag{14c}$$

where $K_j$ is the Kalman gain.

## SEQUENTIAL LINEARIZATION-BASED TARGETING

We propose a sequential linearization-based targeting approach for NRHO station keeping in Algorithm 1 based on the well-known $x$-axis crossing control method.[14] This approach does not require a pre-computed baseline solution like the one in Figure 1. In fact, it can generate one. The key idea behind the algorithm is to test (in Line 11) when the spacecraft arrives near apolune whether the $x$-component of the velocity at a perilune a few revolutions (typically six[14]) downstream is within a certain threshold $\epsilon$. If it is not, then a sequential linearization approach is used to compute a delta-v correction which ensures that the predicted target perilune state of the nonlinear dynamics (4) satisfies the velocity threshold. The proposed approach combines the so called short- and long-horizon maneuvers for station keeping, and reduces vulnerability to accumulation of errors while targeting several revolutions downstream. The typical $x$-axis crossing control computes delta-v corrections based on the state transition matrix (STM) computed for a single predicted trajectory from current apolune to the target perilune. Since the errors due to linearization accumulate over long duration, the calculated delta-v correction might not result in the intended behavior. The strategy we propose iteratively predicts the target perilune state and updates the delta-v until the desired $x$-axis velocity at perilune is achieved according to the nonlinear model (4). Each iteration of the sequential linearization process solves for the minimum-magnitude delta-v correction which ensures that the magnitude of $x$-axis velocity at target perilune does not exceed $\epsilon$ (Line 12). This problem is equivalent to that of determining the projection of the origin in $\mathbb{R}^3$ onto the intersection of two half-spaces. The solution of the projection operation is known in closed-form [37, Proposition 29.23]. Any $y$ satisfying the targeting condition in Line 12 belongs to the intersection of two halfspaces

$$\left\{ y \,\middle|\, \left| a^\top y + b \right| \le \epsilon \right\} \iff \left\{ y \,\middle|\, a^\top y \le \epsilon - b \right\} \bigcap \left\{ y \,\middle|\, -a^\top y \le -\epsilon + b \right\}, \tag{15}$$

where $a^\top = \Phi_{\mathrm{p}}^{[4,4:6]}$ and $b = \dot{x}_{\mathrm{p}}$. Also, observe that when $\epsilon = 0$ Line 12 is equivalent to estimating the projection of the origin onto a subspace. To account for uncertainties with state estimation and system model, the trigger condition is evaluated every time the spacecraft comes close to an apolune. Such a recursive strategy for handling uncertainties obviates the need for separate short-horizon maneuvers to track the solution generated by Algorithm 1.

**Algorithm 1** Sequential Linearization-based Targeting

**Input:** $\widehat{\theta}_0, P_0, K, H, \Delta t, \epsilon$

1: $E_v \leftarrow \begin{bmatrix} 0_{3\times 3} \\ I_3 \end{bmatrix}$
2: **for** $0 \leq k \leq K-1-H$ **do**
3: $\quad \widetilde{k} \leftarrow k + H$
4: $\quad T \leftarrow \left[\widetilde{k} t_{\text{TBP}}, (\widetilde{k}+1) t_{\text{TBP}}\right]$ ▷ *Time interval containing target perilune after H revolutions*
5: $\quad t_{\mathrm{p}} \leftarrow \textsc{SearchPerilune}(\widehat{\theta}_k, T)$ ▷ *Target perilune time instant*
6: $\quad T \leftarrow \left[k t_{\text{TBP}}, t_{\mathrm{p}}\right]$
7: $\quad \theta_{\mathrm{p}} \leftarrow \textsc{Propagate}(\widehat{\theta}_k, T)$ ▷ *Target perilune state*
8: $\quad \Phi_{\mathrm{p}} \leftarrow \text{STM}(\widehat{\theta}_k, T)$ ▷ *Linearize about predicted trajectory to target perilune*
9: $\quad \dot{x}_{\mathrm{p}} \leftarrow \theta_{\mathrm{p}}^{[4]}$ ▷ *$x$-axis velocity at target perilune*
10: $\quad \Delta v_k \leftarrow [0\ 0\ 0]^\top$
11: $\quad$ **while** $\dot{x}_{\mathrm{p}} \geq \epsilon$ **do**
$\quad\quad$ ▷ *Compute minimum-norm delta-v as projection on intersection of two half-spaces*
12: $\quad\quad \Delta v \leftarrow \underset{y\in\mathbb{R}^3}{\text{argmin}} \|y\|_2$ subject to $|\Phi_{\mathrm{p}}^{[4,4:6]} y + \dot{x}_{\mathrm{p}}| \leq \epsilon$
13: $\quad\quad \Delta v_k \leftarrow \Delta v_k + \Delta v$ ▷ *Update delta-v*
14: $\quad\quad \theta_{\mathrm{p}} \leftarrow \textsc{Propagate}(\widehat{\theta}_k + E_v \Delta v_k, T)$ ▷ *Predict target perilune state with delta-v correction*
15: $\quad\quad \Phi_{\mathrm{p}} \leftarrow \text{STM}(\widehat{\theta}_k + E_v \Delta v_k, T)$ ▷ *Linearize about new predicted trajectory*
16: $\quad\quad \dot{x}_{\mathrm{p}} \leftarrow \theta_{\mathrm{p}}^{[4]}$
17: $\quad$ **end while**
18: $\quad T \leftarrow [k t_{\text{TBP}}, (k+1) t_{\text{TBP}}]$
$\quad$ ▷ *Estimate state at next apolune with delta-v correction*
19: $\quad \left(\widehat{\theta}_{k+1}, P_{k+1}\right) \leftarrow \textsc{PropagateFilter}(\widehat{\theta}_k + E_v \Delta v_k, T, \Delta t, P_k)$
20: **end for**
21: $c \leftarrow \sum_{k=0}^{K-1-H} \|\Delta v_k\|_2$ ▷ *Cumulative station-keeping cost*

**Output:** $c,\ \{\Delta v_j\}_{j=0}^{K-1-H}$

The input to Algorithm 1 assumes that the true initial state of the spacecraft is close to an apolune state of a known NRHO baseline solution. An estimate for the initial state $\widehat{\theta}_0$ and the associated covariance $P_0$ are provided as input. It is reasonable to assume that the spacecraft was station-keeping on another baseline solution, and that Algorithm 1 begins execution when the spacecraft reaches the terminal apolune state of that baseline solution. The other inputs to Algorithm 1 are the targeting horizon $H$, which is the number of revolutions downstream until the target perilune, the planning

horizon $K$, which is the total number of revolutions around the Moon for which station keeping is performed, the sampling time $\Delta t$ of the OPNAV measurements, and the threshold $\epsilon$ for targeting the $x$-axis velocity at perilune.

The various components of Algorithm 1 are as follows. The PROPAGATE$(\widehat{\theta}, T)$ function returns the final state of the trajectory predicted by propagating the spacecraft dynamics (4) with initial condition $\theta$ for time interval $T$. The STM$(\theta, T)$ function returns the STM for time interval $T$ of the linear approximation of the system about the trajectory predicted by PROPAGATE$(\theta, T)$. The PROPAGATEFILTER$(\theta, T, \Delta t, P)$ function calls the EKF which accepts OPNAV position measurements at sampling intervals $\Delta t$ to estimate the true spacecraft state at the end of time interval $T$, with initial state $\theta$ and covariance $P$. And finally, the SEARCHPERILUNE$(\theta, t, T)$ function in Line 5 predicts the target perilune time within the interval $T$ via a bisection search for determining the perilune state, where the initial state is $\theta$ at time $t$. Note that it is not critical to apply the maneuvers precisely at apolune. Since the time scale of the dynamics is slow near apolune, we can use the time period $t_{\text{TBP}}$ of the NRHO in CR3BP to approximate the actual apolune time. However, we cannot use such an approximation for predicting the target perilune states due to the fast time scale of the dynamics near perilune. Even a small error in predicting the target perilune time may cause the algorithm to target a state significantly different from the actual perilune which will cause the trajectory to diverge. This is because states far from either perilune or apolune are supposed to have significantly large $x$-axis velocity on a NRHO solution. So targeting them to be close to zero would be incorrect. The SEARCHPERILUNE function ensures that the target perilune state is accurately predicted.

A block diagram of the simulation stack considered in this work with station keeping, state estimation, and OPNAV is shown in Figure 5. The first component of the OPNAV block is described in Figure 2. We do not consider spacecraft attitude control in this work. We assume that the spacecraft camera(s) can be oriented to image the Moon in each sampling period.

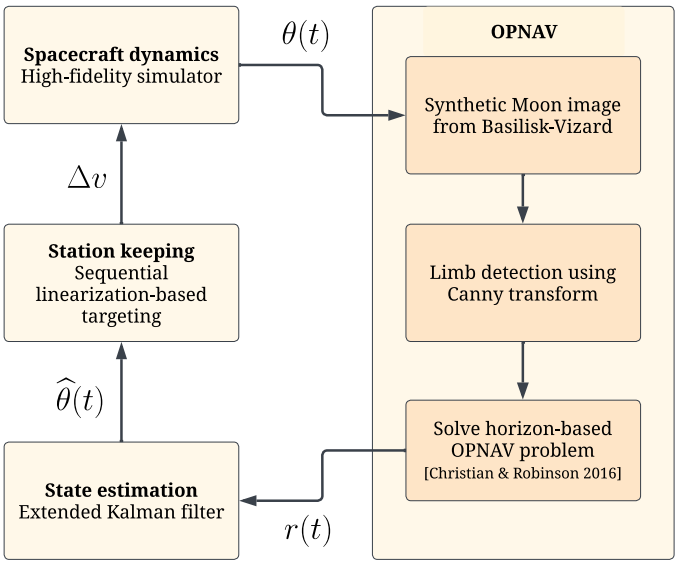


**Figure 5**: Block diagram of the closed-loop station-keeping simulator with OPNAV.

## RESULTS

This section presents the results of station keeping on NRHO from the closed-loop simulation described in Figure 5.

Figure 6 shows the error in state estimates from the EKF that receives OPNAV measurements at sampling intervals of 3 hours for a spacecraft that followed a known NRHO baseline solution for 26 days. The $2\sigma$ bounds on measurements and state estimates are shown as red and blue patches respectively. The true initial state is an apolune state of the baseline solution. The initial state estimate for the filter is obtained by randomly perturbing the true position by $5$ km and true velocity by $5$ cm $\text{s}^{-1}$. The initial state covariance is a diagonal matrix chosen to be consistent with the initial state error. The high sensitivity of the spacecraft dynamics near perilune leads to relatively large state estimation error. The spikes of about $40$ cm $\text{s}^{-1}$ prominently seen in the error in velocity estimates in Figure 6 correspond to perilune. Hence, perilune is unsuitable for applying delta-v corrections. However, the velocity estimation error near the apolune region is relatively lower at around 1 cm $\text{s}^{-1}$, which allows maneuvers to be executed effectively.

Furthermore, the measurement error along $z$-axis in Figure 6 is significantly higher than the error along the other two axes. This is partly due to the fact that the boresight direction of the spacecraft camera is closely aligned with the $z$-axis for a significant duration in each revolution of the NRHO, in particular when the spacecraft is close to apolune and perilune. It is well-known that in horizon-based OPNAV there is larger measurement uncertainty in the camera boresight direction.[38]

Given the sensitivity of the spacecraft dynamics, it is possible for the estimated and true states to diverge away after a large delta-v correction ($\sim 5$ cm $\text{s}^{-1}$) if the filter trusts the predicted state too much without accounting for the discontinuous change in state after the impulse. Therefore, we re-initialize the state covariance matrix to the value at the start of the simulation each time the magnitude of the computed delta-v correction exceeds a specified threshold (1 cm $\text{s}^{-1}$).

Figure 8 shows the states estimates and OPNAV measurements for a 1-year station-keeping simulation obtained using Algorithm 1. The OPNAV measurements are obtained at 6 hr intervals. The tolerance $\epsilon$ on the target perilune $x$-axis velocity is $20$ m $\text{s}^{-1}$. The estimation error at the apolune region (where the maneuvers are applied) is roughly $1$ km in position and $1$ cm $\text{s}^{-1}$ in velocity. The annual station-keeping cost for this simulation is $114.06$ cm $\text{s}^{-1}$. Repeating the simulation with variations in the initial state estimate given to the the filter results in similar station-keeping cost. In comparison to the relevant NRHO station-keeping result with OPNAV reported for the medium-error quiet spacecraft case in [12, Table 7], the result from the proposed approach requires significantly lower annual delta-v. The cumulative delta-v as a function of time, shown in Figure 8a, increases gradually without large jumps, which is desirable for the reliability and safety of the approach.

## CONCLUSION

We proposed a targeting-based approach for station keeping on the near rectilinear halo orbit (NRHO) chosen for the Lunar Gateway and demonstrated it in a closed-loop simulation with a state estimator which receives spacecraft position measurement from horizon-based optical navigation (OPNAV). We use the astrodynamics simulation and visualization software Basilisk and Vizard for generating realistic OPNAV measurements from synthetic images of Moon which accurately show the limb formed on the Moon horizon due to illumination from the Sun. The proposed approach is able to deliver an annual station-keeping cost close to $1.14$ m $\text{s}^{-1}$, and it is robust to measurement uncertainty of about $10$ km observed with OPNAV measurements on the NRHO trajectory.

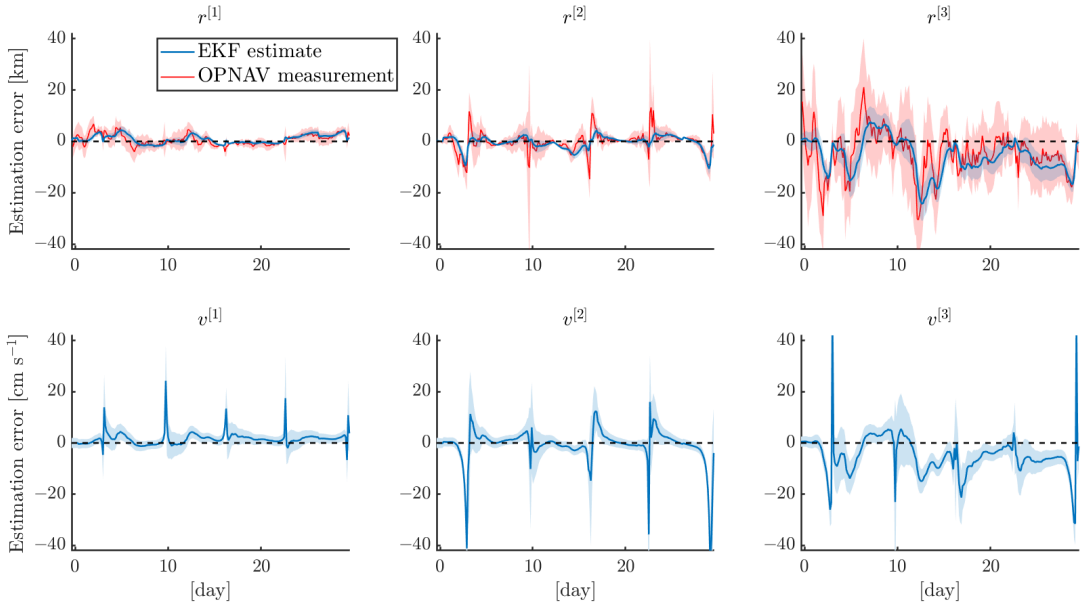


**Figure 6**: EKF state estimation error with OPNAV measurements provided at 3 hour intervals for a spacecraft that follows a NRHO baseline solution for 26 days. The $2\sigma$ bands for the OPNAV position measurement (red) and state estimate (blue) are shown.

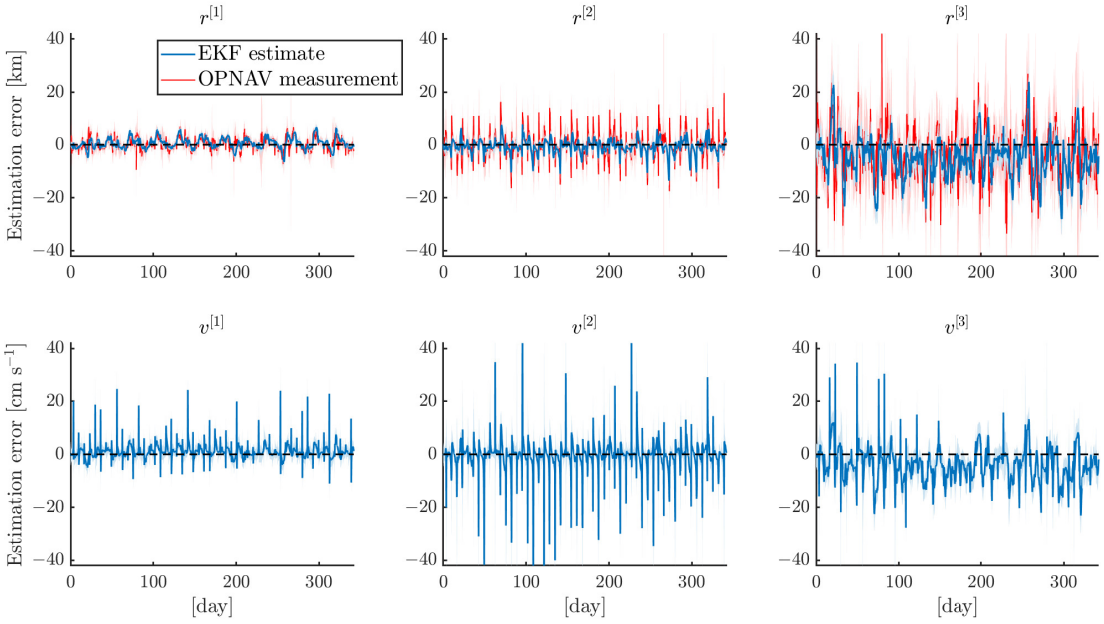


**Figure 7**: The state estimation error for a 1-year closed-loop station-keeping simulation with OPNAV measurements. The $2\sigma$ bands for the OPNAV position measurement (red) and state estimate (blue) are shown.

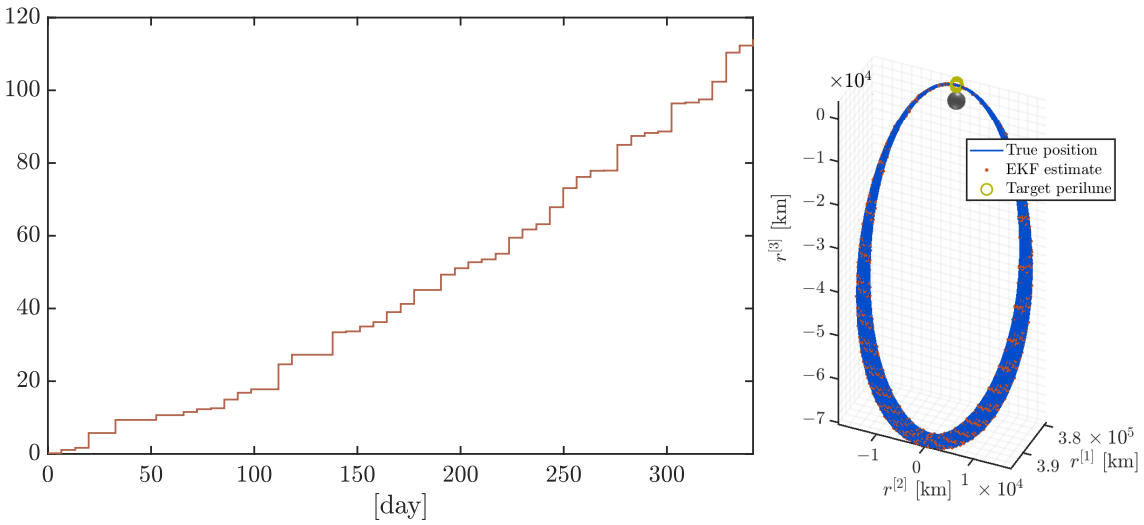


(a) Cumulative delta-v = 114.06 cm $s^{-1}$.

(b) Position trajectory.

**Figure 8**: Station keeping with OPNAV measurements.

Future work will improve the simulator to make the computation of OPNAV measurement covariance more reliable, and specialize the design of the filter to exploit the dynamical features of a high-fidelity NRHO solution to reduce the state estimation error at perilune, which will potentially contribute to a reduction in the annual station-keeping cost. The robustness and efficiency of the station-keeping approach with DSN and OPNAV measurements will be compared. In addition, the performance of the proposed approach adapted with short-horizon maneuvers will be examined.

## NOTATION

| | |
|---|---|
| $I_n$ | $n \times n$ identity matrix |
| $x^{[j]}$ | $j$th entry of vector $x$ |
| $x^{[j:k]}$ | vector formed by $j$th through $k$th entries of vector $x$ |
| $Y^{[i,j:k]}$ | vector formed by entries from columns $j$ through $k$ of the $i$th row of matrix $Y$ |

## REFERENCES


[1] K. C. Laurini, B. Hufenbach, J. Hill, and A. Ouellet, "The Global Exploration Roadmap and Expanding Human/Robotic Exploration Mission Collaboration Opportunities," IAF 66th International Astronautical Congress, October 2015, pp. 1–9.

[2] B. Hufenbach, K. Laurini, N. Satoh, C. Lange, R. Martinez, J. Hill, M. Landgraf, and A. Bergamasco, "International Missions to Lunar Vicinity and Surface - Near-Term Mission Scenario of the Global Space Exploration Roadmap," IAF 66th International Astronautical Congress, October 2015, pp. 1–11.

[3] D. Lee, "Gateway Destination Orbit Model: A Continuous 15 Year NRHO Reference Trajectory," tech. rep., NASA Johnson Space Center, 2019.

[4] M. Duggan, X. Simon, and T. Moseman, "Lander and cislunar gateway architecture concepts for lunar exploration," 2019 IEEE Aerospace Conference, IEEE, 2019, pp. 1–9.

[5] "What is CAPSTONE?," *https://www.nasa.gov/directorates/spacetech/small_spacecraft/capstone*. Accessed: April 29, 2022.

[6] "Further Details on Communications Issues with NASA's CAPSTONE," *https://blogs.nasa.gov/artemis/2022/07/05/further-details-on-communications-issues-with-nasas-capstone/*. Accessed: July 5, 2022.

[7] "Mission Team Determines Cause of Communications Issues for NASA's CAPSTONE," *https://blogs.nasa.gov/artemis/2022/07/07/mission-team-determines-cause-of-communications-issues-for-nasas-capstone/*. Accessed: July 7, 2022.

[8] J. J. Parker, F. Dovis, B. Anderson, L. Ansalone, B. Ashman, F. H. Bauer, G. D'Amore, C. Facchinetti, S. Fantinato, G. Impresario, et al., "The Lunar GNSS Receiver Experiment (LuGRE)," Proceedings of the 2022 International Technical Meeting of The Institute of Navigation, 2022, pp. 420–437.

[9] "Teams Press Ahead Toward Artemis I Launch in Late August," *https://blogs.nasa.gov/artemis/2022/07/22/teams-press-ahead-toward-artemis-i-launch-in-late-august/*. Accessed: July 22, 2022.

[10] D. C. Folta, T. A. Pavlak, A. F. Haapala, K. C. Howell, and M. A. Woodard, "Earth–Moon libration point orbit stationkeeping: Theory, modeling, and operations," Acta Astronautica, Vol. 94, Jan 2014, p. 421–433, 10.1016/j.actaastro.2013.01.022.

[11] L. Bucci, M. Lavagna, and R. Jehn, "Station keeping techniques for near rectilinear orbits in the Earth–Moon system," Proceedings of 10th international ESA conference on GNC systems, Salzburg, Austria, Vol. 29, 2017.

[12] D. C. Davis, S. Bhatt, K. Howell, J.-W. Jang, R. Whitley, F. Clark, D. Guzzetti, E. Zimovan, and G. Barton, "Orbit maintenance and navigation of human spacecraft at cislunar near rectilinear halo orbits," AAS/AIAA Space Flight Mechanics Meeting, 2017.

[13] D. C. Davis, S. M. Phillips, K. C. Howell, S. Vutukuri, and B. P. McCarthy, "Stationkeeping and transfer trajectory design for spacecraft in cislunar space," AAS/AIAA Astrodynamics Specialist Conference, 2017, p. 1–20.

[14] D. Guzzetti, E. M. Zimovan, K. C. Howell, and D. C. Davis, "Stationkeeping analysis for spacecraft in lunar near rectilinear halo orbits," 27th AAS/AIAA Space Flight Mechanics Meeting, American Astronautical Society San Antonio, Texas, 2017, p. 1–20.

[15] C. P. Newman, D. C. Davis, R. J. Whitley, J. R. Guinn, and M. S. Ryne, "Stationkeeping, Orbit Determination, and Attitude Control for Spacecraft in Near Rectilinear Halo Orbits," AAS Astrodynamics Specialists Conference, 2018.

[16] X. Fu, N. Baresi, and R. Armellin, "A High-order Target Point Approach to the Stationkeeping of Near Rectilinear Halo Orbits," 71th International Astronautical Congress, CyberSpace Edition, University of Surrey, 2020.

[17] V. Muralidharan, A. Weiss, and U. Kalabić, "Control Strategy for Long-Term Station-Keeping on Near-Rectilinear Halo Orbits," AIAA Scitech 2020 Forum, 2020, 10.2514/6.2020-1459.

[18] V. Muralidharan and K. C. Howell, "Stationkeeping in Earth-Moon Near Rectilinear Halo Orbits," AAS/AIAA Astrodynamics Specialist Conference, South Lake Tahoe, California, USA, 2020.

[19] X. Fu, N. Baresi, and R. Armellin, "Stochastic Optimization for Stationkeeping of Near Rectilinear Halo Orbits Using a High-order Target Point Approach," AAS/AIAA Astrodynamics Specialist Conference, Big Sky, 2021.

[20] P. Elango, S. Di Cairano, U. Kalabić, and A. Weiss, "Local Eigenmotion Control for Near Rectilinear Halo Orbits," 2022 American Control Conference (ACC), 2022, pp. 1822–1827.

[21] K. C. Howell and T. M. Keeter, "Station-keeping Strategies for Libration Point Orbits: Target Point and Floquet Mode Approaches," Spaceflight Mechanics, 1995, pp. 1377–1396.

[22] G. Gómez, K. Howell, J. Masdemont, and C. Simó, "Station-keeping strategies for translunar libration point orbits," Advances in Astronautical Sciences, Vol. 99, No. 2, 1998, pp. 949–967.

[23] D. Malyuta, T. P. Reynolds, M. Szmuk, T. Lew, R. Bonalli, M. Pavone, and B. Açıkmeşe, "Convex Optimization for Trajectory Generation," IEEE Control Systems Magazine (accepted), 2021.

[24] P. W. Kenneally, S. Piggott, and H. Schaub, "Basilisk: A flexible, scalable and modular astrodynamics simulation framework," Journal of aerospace information systems, Vol. 17, No. 9, 2020, pp. 496–507.

[25] J. Wood, M. C. Margenet, P. Kenneally, H. Schaub, and S. Piggott, "Flexible Basilisk astrodynamics visualization software using the Unity rendering engine," AAS Guidance and Control Conference, Breckenridge, CO, 2018.

[26] V. Franzese, S. Ceccherini, K. V. Mani, P. Di Lizia, and F. Topputo, "Feasibility Assessment of Autonomous Optical Navigation in LUMIO Mission," 69th International Astronautical Congress (IAC 2018), International Astronautical Federation, IAF, 2018, pp. 1–6.

[27] G. N. Holt, C. N. D'Souza, and D. W. Saley, "Orion Optical Navigation Progress Toward Exploration Mission 1," 2018 Space Flight Mechanics Meeting, 2018, p. 1978.

[28] T. Teil, S. Bateman, and H. Schaub, "Closed-Loop Software Architecture for Spacecraft Optical Navigation and Control Development," The Journal of the Astronautical Sciences, Vol. 67, No. 4, 2020, pp. 1575–1599.

[29] T. Teil, H. Schaub, and D. Kubitschek, "Centroid and Apparent Diameter Optical Navigation on Mars Orbit," Journal of Spacecraft and Rockets, Vol. 58, No. 4, 2021, pp. 1107–1119.

[30] T. A. Pavlak, Trajectory design and orbit maintenance strategies in multi-body dynamical regimes. PhD thesis, Purdue University, 2013.

[31] V. Muralidharan, Stretching Directions in Cislunar Space: Stationkeeping and an Application to Transfer Trajectory Design. PhD thesis, Purdue University, 2021.

[32] J. A. Christian and S. B. Robinson, "Noniterative Horizon-Based Optical Navigation by Cholesky Factorization," Journal of Guidance, Control, and Dynamics, Vol. 39, No. 12, 2016, pp. 2757–2765.

[33] W. M. Folkner, J. G. Williams, and D. H. Boggs, "The Planetary and Lunar Ephemeris DE 421," IPN progress report, Vol. 42, No. 178, 2009, pp. 1–34.

[34] J. Canny, "A computational approach to edge detection," IEEE Transactions on Pattern Analysis and Machine Intelligence, No. 6, 1986, pp. 679–698.

[35] G. Bradski, "The OpenCV Library," Dr. Dobb's Journal of Software Tools, 2000.

[36] A. Gelb and The Analytic Sciences Corporation, Applied Optimal Estimation. MIT Press, 1974.

[37] H. H. Bauschke and P. L. Combettes, Convex Analysis and Monotone Operator Theory in Hilbert Spaces, Vol. 408. Springer, 2011.

[38] J. A. Christian, "A tutorial on horizon-based optical navigation and attitude determination with space imaging systems," IEEE Access, Vol. 9, 2021, pp. 19819–19853.